



This is a repository copy of *Surface defect evolution in hot rolling of high-Si electrical steels* .

White Rose Research Online URL for this paper:
<http://eprints.whiterose.ac.uk/117657/>

Version: Accepted Version

Article:

Nioi, M., Celotto, S., Pinna, C. et al. (2 more authors) (2017) Surface defect evolution in hot rolling of high-Si electrical steels. *Journal of Materials Processing Technology*, 249. pp. 302-312. ISSN 0924-0136

<https://doi.org/10.1016/j.jmatprotec.2017.06.017>

Reuse

This article is distributed under the terms of the Creative Commons Attribution-NonCommercial-NoDerivs (CC BY-NC-ND) licence. This licence only allows you to download this work and share it with others as long as you credit the authors, but you can't change the article in any way or use it commercially. More information and the full terms of the licence here: <https://creativecommons.org/licenses/>

Takedown

If you consider content in White Rose Research Online to be in breach of UK law, please notify us by emailing eprints@whiterose.ac.uk including the URL of the record and the reason for the withdrawal request.



eprints@whiterose.ac.uk
<https://eprints.whiterose.ac.uk/>

Surface Defect Evolution in hot rolling of High-Si Electrical Steels

Nioi¹, M., Celotto², S., Pinna¹, C., Swart², E., Ghadbeigi¹, H.

¹Department of Mechanical Engineering, The University of Sheffield, Sheffield, UK

²Tata Steel Europe R&D, IJmuiden, The Netherlands

CORRESPONDING AUTHOR DETAILS:

Full name: Nioi Manuel

Email address: Mnioi1@sheffield.ac.uk

Full postal address: Mining block, Room RC08, Sir Frederick Mappin Building, Sheffield, S1 3JD, UK

ABSTRACT

Surface defects on metal strip products can have their root cause created in the hot rolling process by cavities and indents entrapped scale. The initial size and aspect ratio of surface features are critical parameters that determine whether they will be eliminated by the rolling process. The present research investigates the effects of the initial cavity geometry and the evolution mechanisms in a single hot rolling pass for a high-silicon electrical steel substrate. Laboratory hot-rolling experiments were carried out on blocks with open cavities of different geometries machined into the surface. The final geometry of the longitudinal and transversal profiles of the deformed cavities was analysed from metallurgical cross-sections. For a given initial cavity width, the width of the resulting oxide-filled defect is inversely related to the initial depth of the machined cavity. It has also been observed that the depth of defects increases linearly with the original depth to width aspect ratio of the initial cavities. Cavities with a depth of less than 1 mm essentially disappeared after the rolling. The final length is only dependent on its initial length in the rolling direction. The

percentage reduction of cross-sectional area of the defects is found to increase with the initial depth and width of the cavities.

Key Words: Hot Rolling, Surface Defect, Electrical steel, Deformation, Oxide

1. INTRODUCTION

Hot rolling is a key process step to transform cast or semi-finished steels into finished products. The obtained surface integrity is important for thin strip applications. Electrical steels are produced using a hot-rolled strip of 2-3 mm gauge that is then cold rolled to the final product with a thickness of a few hundreds of micrometres. Hot-rolled strips are produced from slabs that are heated up to 1100-1400°C prior to the first rolling stage. The heating process in the furnace and the time between individual passes results in the formation and growth of surface oxide layers. The presence of the surface oxide scale affects the roll bite tribology in the rolling mills as shown by studies regarding its effect on interfacial friction in hot rolling (Munther and Lenard, 1999), friction coefficient during hot rolling of low-carbon steels (Lenard and Barbulovic-nad, 2002), oxide scale behaviour during rolling (Krzyzanowski et al., 2009), measurements of friction during hot rolling carried out on aluminium strips (Hum et al., 1996) and boundary conditions in hot and cold flat rolling (Lenard, 1990).

Although high-pressure water-jet spray is used to remove oxide scales, remnants can be trapped in surface cavities of certain geometrical characteristics and/or aspect ratios. Surface defects with embedded oxide scales are deformed as a result of subsequent rolling operations to achieve the required final strip thickness. The scale and surface features may heavily deform due to the rolling induced plastic deformation, resulting in centimetres to metres long surface defects in the finished products, as shown by the experiments and simulations carried out by Lee (Lee S.-L., 2008). These surface defects can interfere with the performance of the final product. It is therefore important to understand the formation and evolution of these type of surface features during hot rolling of thin sheet metals, with the ultimate aim to prevent their formation or at least control their evolution during the hot-rolling process.

Few important studies have been made to better understand the evolution mechanisms and predict the formation of surface defects in hot-rolling operations. In these two studies, the variation in the initial feature geometries was limited to two principal dimensions as defects were axially symmetric holes. This may not capture the three-dimensionality of deformation mechanisms involved in its evolution. Lee and Choi (Lee S.-L., 2008) studied the evolution of artificial surface cavities fabricated by drilling cylindrical holes into the surface of slabs of a low carbon steel for multi-pass hot rolling experiments. A range of diameter to depth ratios was used to investigate effects of initial cavity size on the final geometry to determine the critical aspect ratio that leads to formation of concealed surface defects. A similar approach was used in the literature (Záhumenský and Merwin, 2008), where again, drilled holes were used as artificial imperfections on the surface of cast slabs of a generic tin-grade steel to study the cavity deformation during a multi-stand hot-rolling process. A threshold value is reported in (Záhumenský and Merwin, 2008), for the initial depth of the cavities, above which the features cannot be removed by plastic deformation due to the hot-rolling operation applied. It is also concluded that the possibility of surface cavity elimination increases for features with smaller initial depth. Similar results were also reported in (Zeze et al., 2001) for hot rolling tests carried out on cast steel slabs containing surface artificial defects of different dimensions. The geometry of the initial cavities was found to be one of the critical factors for their elimination by further rolling steps as reported in (Shainu et al., 2008). With regards to the movement of defects during rolling, it is found to be associated with the lateral spreading of the material (Moir and Preston, 2002).

To the best knowledge of the authors, there is still a lack of understanding about surface defect evolution mechanisms during rolling, particularly for high-Si electrical steels. The available literature shows that only cylindrical features were analysed for different materials with very limited analysis on the effect of the aspect ratio in different directions because of the axial-symmetry of the studied features. There are only few studies using experimental approach to investigate the evolution of cracks during hot rolling. (Yu et al., 2008) studied the elongation of an initial crack during rolling for

each rolling reduction stand. It is also reported that large deformations promote the closing of the initial cracks, but not its elimination (Vlado et al., 2011).

The present research aims to study evolution mechanisms of surface cavities during the hot-rolling of a high-silicon electrical steel substrate with approximately 40% thickness reduction, an amount that is typical for the first rough pass. Surface cavities with different sizes and aspect ratios were defined to represent three-dimensional deformation conditions. A parametric study was used to investigate the effects of initial geometry on the final cavity shape and dimensions. An analytical model was also developed to represent and predict the final defect dimensions with respect to the initial surface cavity geometry.

2. EXPERIMENTS

Cavities with different parametric dimensions (as shown in Figure 1) were designed based on the measurements of surface indentations from rejected production continuous-cast slabs of 3 wt% silicon grain-oriented electrical steel. The length (L), width (W) and depth (D) dimensions were used as the control parameters to determine different aspect ratios of the designed cavities. Three different values were selected for each of the control parameters to represent the full range of surface defects lengths, width and depths measured.

The characterisation of the surface topography revealed a very small average depth of about 0.5 mm with only a few deep indentations found in the slabs, but the largest measured values were used to ensure the worst case conditions were covered. Consequently, 1mm, 3mm and 5mm were selected for the depth parameter (D). The three length and width levels were selected as extremes and mean values of the range of dimensions which included the full range of width and length of the defects observed. The matrix of experimental dimensions of the surface cavities are shown in Table 1. The corner radius was about 0.5 mm, which was determined by the milling tool radius.

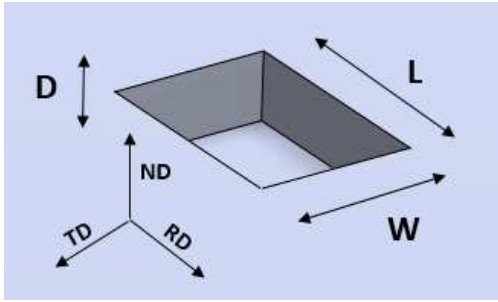


Figure 1: Parameters used to describe the initial surface cavity geometry

Table 1: Cavity identification code list and corresponding dimensions

DEFECT		A 1	B 1	C 1	D 1	E 1	F 1	G 1	H 1	I 1	A 2	B 2	C 2	D 2	E 2	F 2	G 2	H 2	I 2	A 3	B 3	C 3	D 3	E 3	F 3	G 3	H 3	I 3	
D (mm)	1	X	X	X	X	X	X	X	X	X																			
	3										X	X	X	X	X	X	X	X	X										
	5																			X	X	X	X	X	X	X	X	X	X
W (mm)	3	X	X	X							X	X	X							X	X	X							
	7							X	X	X							X	X	X							X	X	X	
	11				X	X	X							X	X	X							X	X	X				
L (mm)	4	X			X			X			X			X			X			X			X			X			
	10		X			X			X		X			X				X			X			X			X		
	17			X			X			X		X			X			X				X			X			X	

The material used for the experiments was the same grain-oriented electrical steel wherein the surface defects were observed, with a nominal chemical composition of Fe-3.1wt%Si-0.05wt%C-0.2wt%Mn and minor additions of Cu, S, Al and Sn (<0.1 wt% individually). Six rectangular blocks 115mm x 85mm x 25mm in size were cut from the 70mm thick production cast slabs. These were sectioned parallel to the rolling-plane at the mid-thickness and then machined from both rolling-plane surfaces down to final thickness of 25 mm (note that the initial rough and oxidised slab surface has also been removed). The microstructure of the block consists of columnar grains extending through the whole thickness as is typical for as-cast microstructures of these materials, giving the isotropic properties in the rolling plane. The devised cavities were machined into the top surface of the sections (Figure 2). The cavities were positioned to maximise the distance between adjacent cavity boundaries and the block edges to minimise interactions between the deformation fields.

The experiments were conducted on a laboratory mill with roll diameters of 223mm. A muffle furnace capable of reaching temperatures of 1400°C placed adjacent to the roll was used to heat the samples. The heating and cooling practice of the blocks prior to rolling is based on process conditions used for what is called thin-slab low-temperature re-heating for electrical steel industrial production, although much shorter soak times were implemented in the experiments. The blocks were heated in the muffle furnace without protective atmosphere to 1150°C and soaked for 15 minutes at this temperature prior to rolling to homogenise the temperature and to create a primary oxide scale on the surfaces. The blocks were then cooled, predominately by radiation to the surrounding, down to 1050°C within 20 seconds to emulate the heat loss that occurs in production for a slab between exiting the furnace and entering the first roughing mill. The oxide layer was manually scraped off using a flat steel tool before pushing the sections into the rolling gap in the laboratory mill. The rolling operation was then performed at the velocity of 0.035m/s to obtain a 40% thickness reduction in a single rolling pass.

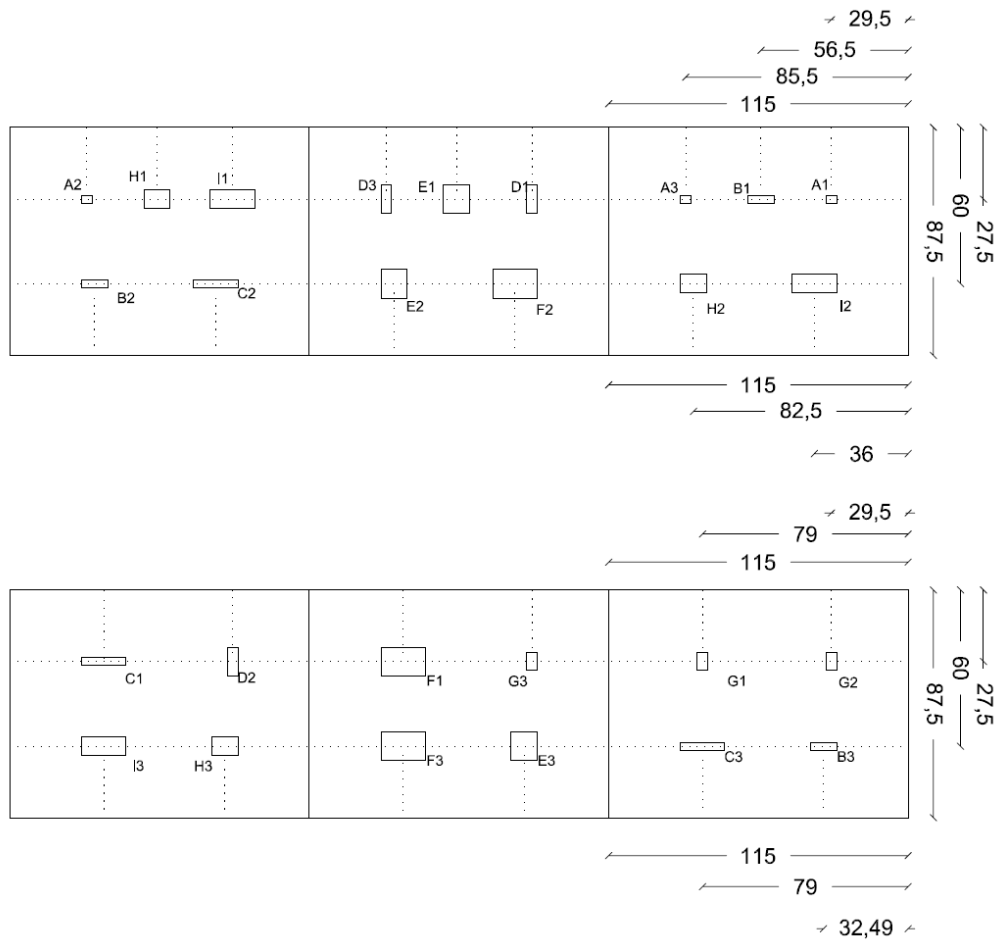


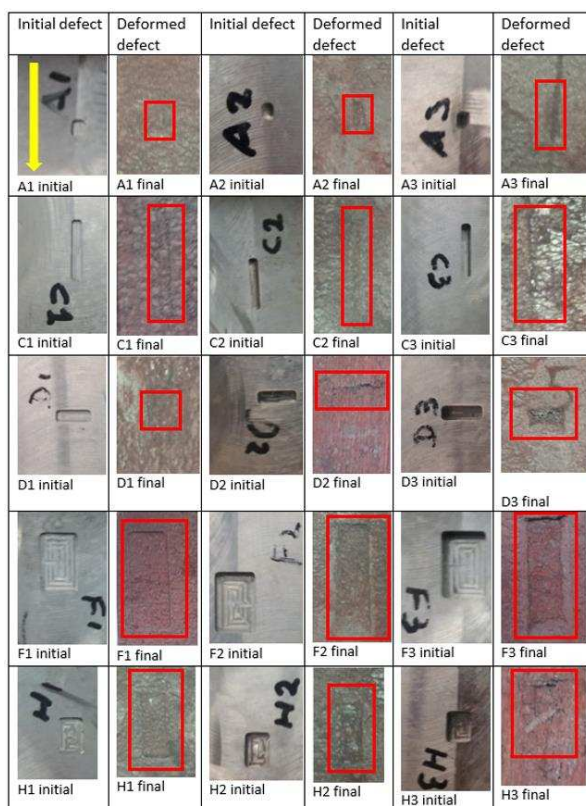
Figure 2: Machined surface cavities on the surface of blocks before the hot rolling operation.

The term “cavity” will be used to refer to the artificial holes drilled into the blocks before rolling and “defect” will be used to refer to the deformed features after the rolling. The top surface of the rolled sections was analysed after the experiments to characterise final cavity geometries. Metallurgical cross-sections of longitudinal and transversal profiles of the final defects were analysed to study the effects of the initial configuration on the deformed geometries and identify the most critical dimensional parameters.

3. RESULTS

The defects were analysed to study the evolution mechanisms. A top view of a subset of 15 defects with five different length (L) to width (W) aspect ratios (0,36; 1,33; 1,43; 1,55; 5,67) and three

different initial depths (1mm, 3mm, 5mm) are presented and compared with the original cavities shape and size before the rolling in Figure 3. The aspect ratios selected to be presented first are those with the minimum and maximum W and L measured and H1-H3 have mean W and L values. The arrow in top-left of Figure 3 indicates the rolling direction for all the images. By comparing the initial cavities and the final defects from the top view in Figure 3, it is noticeable that not only are the defects elongated as expected, but they are also significantly reduced in width from the rolling operation.



10 mm

Figure 3: Optical photographs of the selected cavities and deformed defects (highlighted by red rectangles) on the surface of the rolled blocks

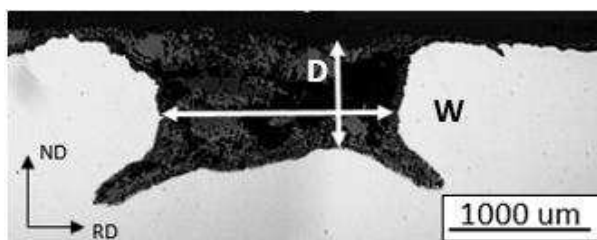


Figure 4: Depth and width measurement scheme

The length of the rolled defects was measured directly from the surface of the rolled blocks and micrographs of each defect in the transverse cross-section were prepared to determine D and W parameters after the rolling induced deformation. The depth was measured at the shallowest point and the width measurement was taken from the narrowest section of the oxide-filled deformed defect as shown in Figure 4. The summary of the measured values for different initial machined cavities is shown in Figure 5. Selected final lengths (Figure 5a-c) of the cavities are colour coded with black, blue, and red representing defects with an initial length of 17mm, 10 mm and 4 mm, respectively. The selected depths of each set of defects are indicated by a marker with different geometries. Similar conventions are used in Figure 5d-f and Figure 5g-l to present the final width and depth, respectively.

The results show that the cavities were elongated in the rolling direction (Figure 5a-c) and reduced in depth (Figure 5g-i) and width (Figure 5d-f) after the rolling operation, as is expected. The initial length was found to be the main geometric parameter that affects the elongation of the surface cavities, for the given reduction ratio, which is also as expected. Cavities with different depth and width and equal length (Figure 5a-c) show similar elongation due to the rolling induced plastic deformation. Additionally, for a given initial depth, the wider cavities evolve to shallower final defects, while deeper resulting defects are formed from cavities with smaller width (Figure 5g-i). It was observed that cavities with depth of 1mm were almost completely eliminated by the process. This is regardless of the initial length of the surface cavities and it is more pronounced for wider initial features (Figure 5i). The dark colour within surface features D3, F3, A3 (Figure 3) are due to the presence of thicker oxide layers in the cavities compared with the original upper surface of the rolled sections.

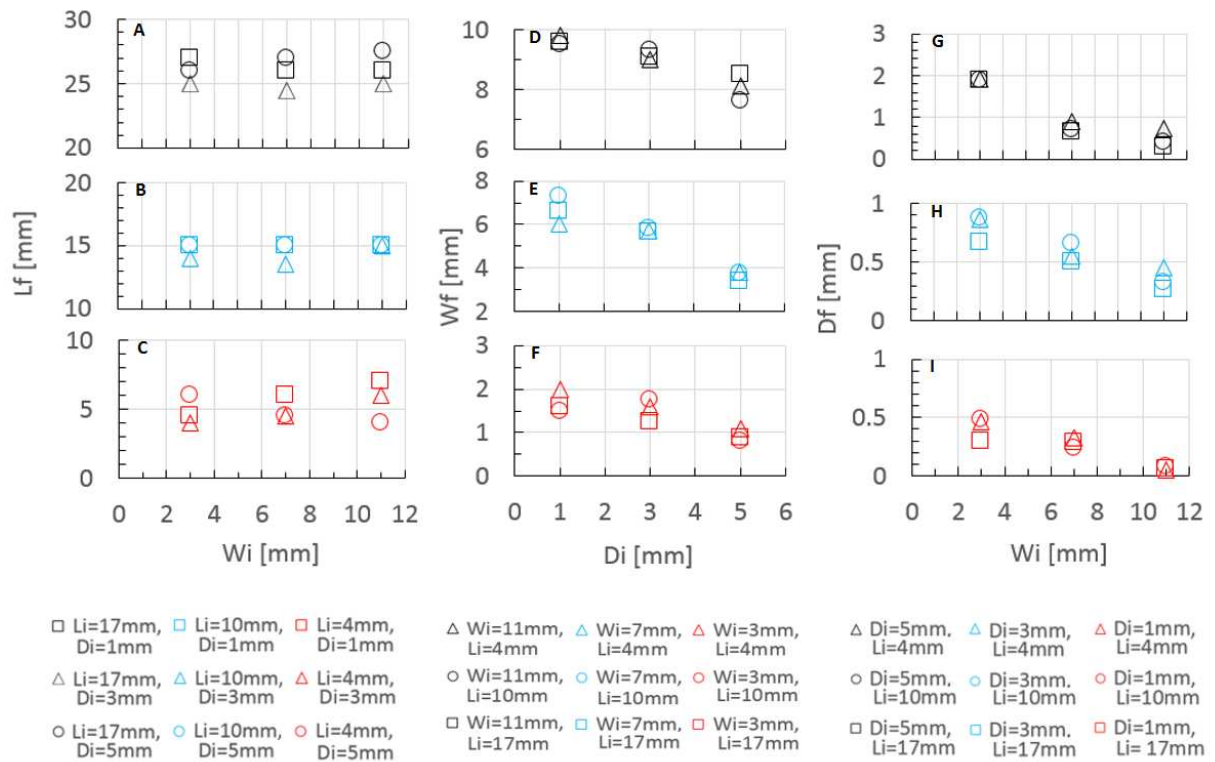


Figure 5: Cavity dimensions, before and after rolling

Micrographs of the defects showing the most representative deformation trends (B3, D3, B2, and G3) in the longitudinal and transverse cross-sections were taken at the mid-planes of the defects as indicated in Figure 6 for a general cavity. These are used to explain the defect formation mechanisms in the next sections.

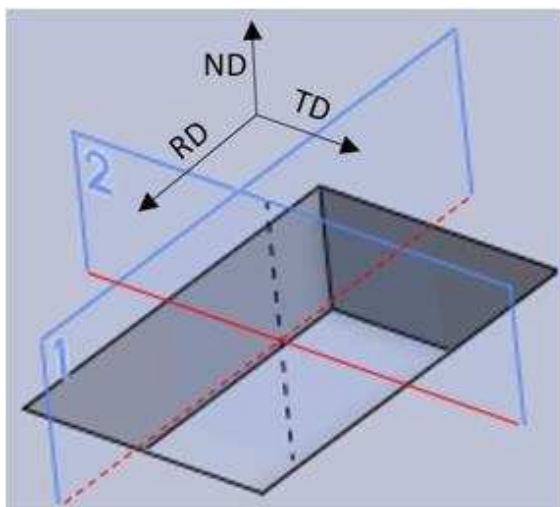


Figure 6: Schematic of the longitudinal (1) and transversal (2) mid sections of the cavities before the rolling process.

Micrographs of Figure 7a-d show the transverse section of the defects, while the micrographs of Figure 7e-h show the longitudinal cross-section of the same defects. The rolling direction is indicated by the arrow in Figure 7e. The defects were found to be partially or completely filled with oxide. The differences are due to the fact that part of the oxide may have fallen out during the preparation and/or handling of the rolled blocks. The micrographs of the transversal section show a lateral deformation in the transverse direction together with the buckling of the side walls resulting in substantial width reduction of the cavities. The micrographs of longitudinal cross-section show that the back side of the defects (i.e. the last side to exit the rolling gap), as it is highlighted by the broken line at the left-hand side of the figures, are folded followed by significant buckling due to the friction between the roll and the strip surface. Consequently, the remaining oxide scales are entrapped in the crevice formed. On the other hand, the flow of material, as a result of the regions leaving the roll gap, generates further opening of the cavities at the front side shown by the highlighted feature with a solid line. This is sometimes associated with the generation of minor crevices as highlighted by the continuous lines (Figure 7e and Figure 7h).

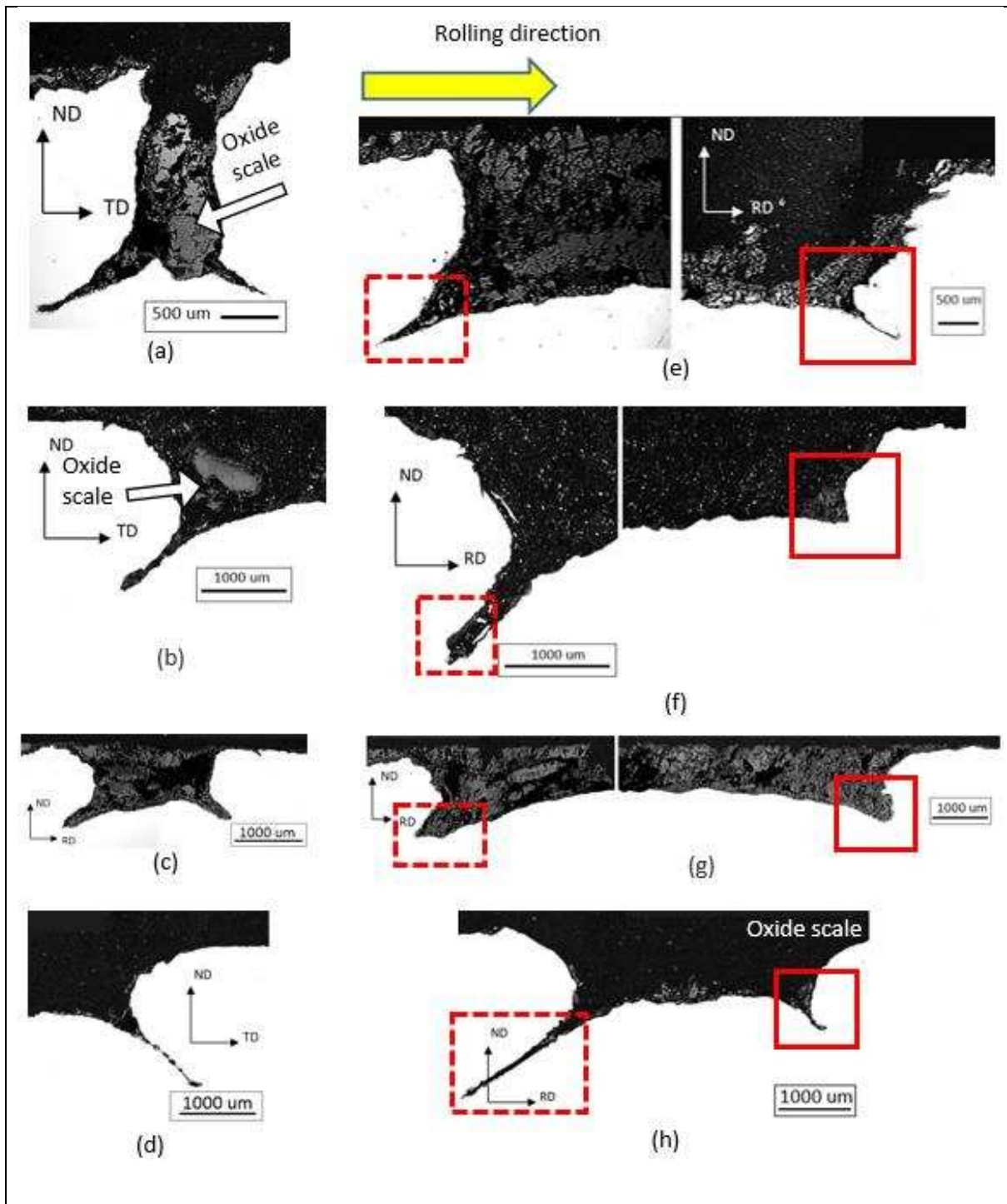


Figure 7: Micrographs of selected defects B3 (a, e), D3 (b, f), B2 (c, g) and G2 (d, h) showing the deformed geometry at the transversal and longitudinal sections as indicated by the respective arrows.

Micrographs of defects B3 and B2 with initial depths of 5mm and 3mm respectively and a width of 3mm, show that cavities with a shallower initial depth show a reduced tendency to create crevices. Conversely, these crevices are more extended for deeper initial cavities (B3 in Figure 7). The crevices

appear in both transversal and longitudinal directions. The micrographs (Figure 7a,c, and g) show that although a scraping technique was used to remove the oxide layer before the rolling operation, there were some oxide scales retained inside the cavities (highlighted by white arrows in Figure 7) and these are buried under the deformed side walls of the cavities. The formation of a larger buckling in the side walls of the defects results in a larger amount of oxide scale to be trapped and buried in the defects. Consequently, the lateral deflection of the side walls, as indicated in Figure 8, can be used as an index to assess the severity of the deformation. This is aligned with the observed deformation behaviour for the cavities with smaller initial depth where a negligible buckling or a complete opening occurs, due to the rolling induced deformation.

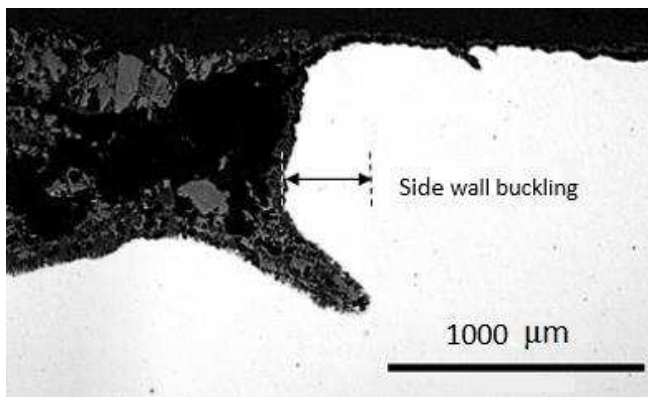


Figure 8: Buckling deformation measurement

Figure 9 presents the measured side wall deflections in order to assess the severity of deformation in the analysed defects. Selected initial widths of the cavities are colour coded with grey, orange and blue representing defects with an initial width of 11mm, 7mm and 3mm, respectively. The measured values show that, for a given initial width, the buckling effect increases with the D/W aspect ratio. This is more pronounced for wider cavities that can be observed from the different slopes of the fitted linear trend lines.

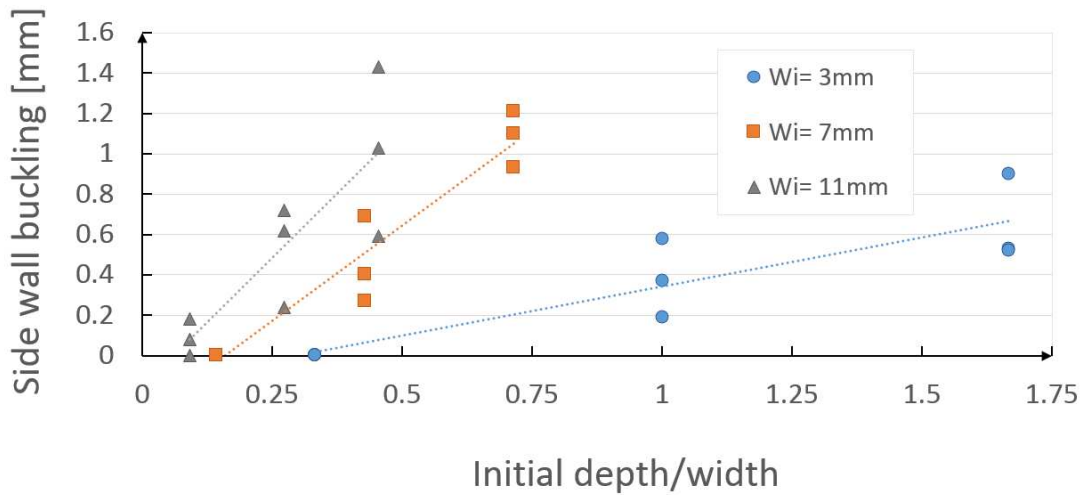


Figure 9: Buckling effect measured for different initial depth/ width (D/W) aspect ratio and initial width (W).

The final depth of the defects can also be used as an index of defect severity as deeper defects are more difficult to eliminate and tend to entrap more oxide. For a more complete description of the depth measurement, it is important to take into account the measured values at the shallowest point of the defect and the depth measured at the deeper corners of the crevices in the defects.

Figure 10 presents the final depth measured at the shallowest point (D_f , coded with triangular marks and different colours depending on the initial depth) and at the crevice corners (D_{fc} , colour coded circular marks and different colour depending on the initial depth) of the defect for given initial depths and initial D/W aspect ratio. The graph shows that for the both measurement criteria for the given initial depths the final depth of the defect increases linearly with the D/W ratio for both the cases. This effect is more evident when the depth is measured at the shallower point.

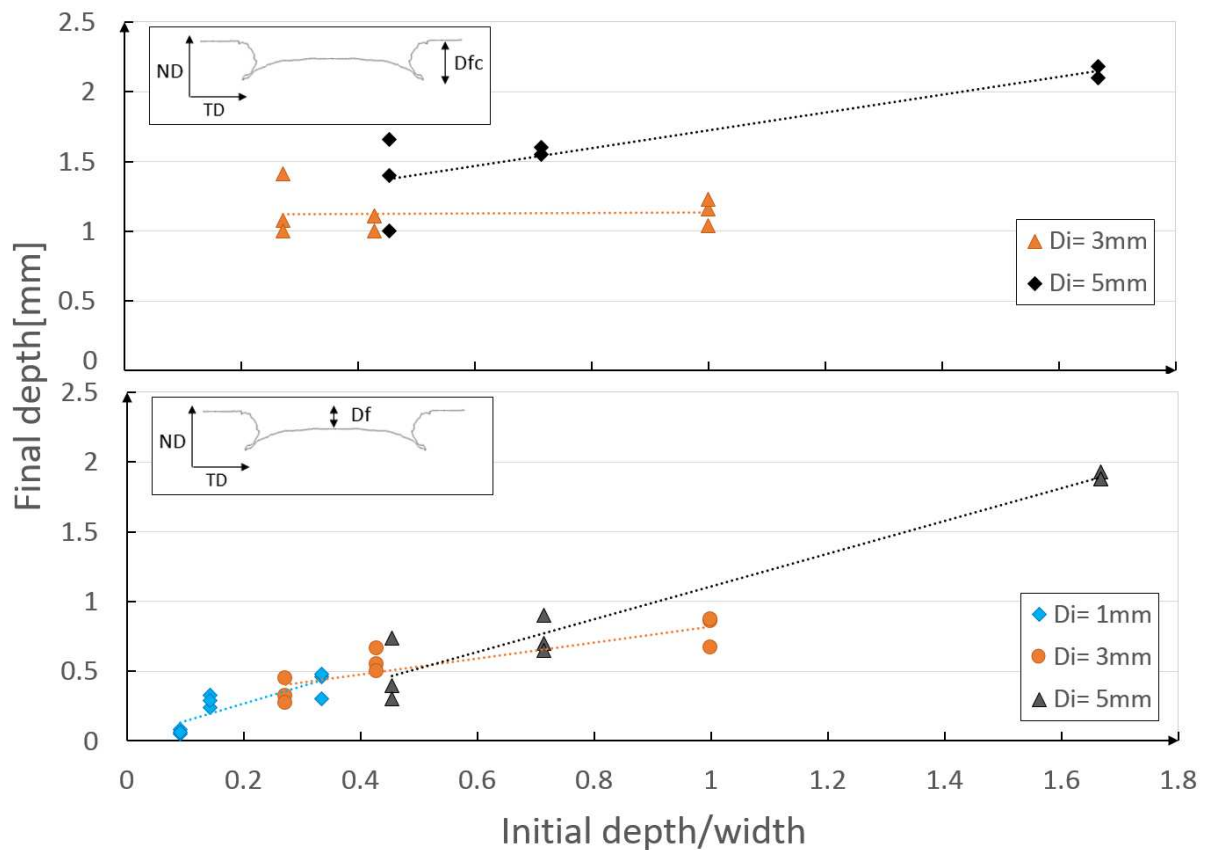


Figure 10: Final defect depth for different initial depth/width ratios and respective trend line.

The reduction of the cavity area is another indication of deformation experienced by the cavities during rolling. This can be found comparing the cross section of the machined cavities with those of deformed defects. Figure 11 shows the cross-sectional area reduction of the cavities made with the same initial widths and different initial depths (Figure 11a) and for cavities made with the same initial depths and different initial widths (Figure 11b). Selected initial widths of the cavities in Figure 11a are colour coded with red, orange and green representing defects with an initial width of 11mm, 7mm and 3mm, respectively. Selected initial depths of the cavities in Figure 11b are colour coded with red, orange and green representing defects with an initial depth of 5mm, 3mm and 1mm, respectively. It can be seen from the graphs that deeper and wider initial cavities are more reduced in terms of percentage of cross-sectional area. In particular, cavities made with the same initial width are more reduced in cross-sectional area if deeper (Figure 11a). Comparable results are found for cavities with same initial depth, they are more reduced in cross-sectional area when wider

(Figure 11b). There are clear indications from these graphs that the increase of the initial depth has a more pronounced effect in terms of percentage reduction of area than the increase of the width of the machined cavities. This is noticeable comparing the different slopes of the trend lines of the two graphs.

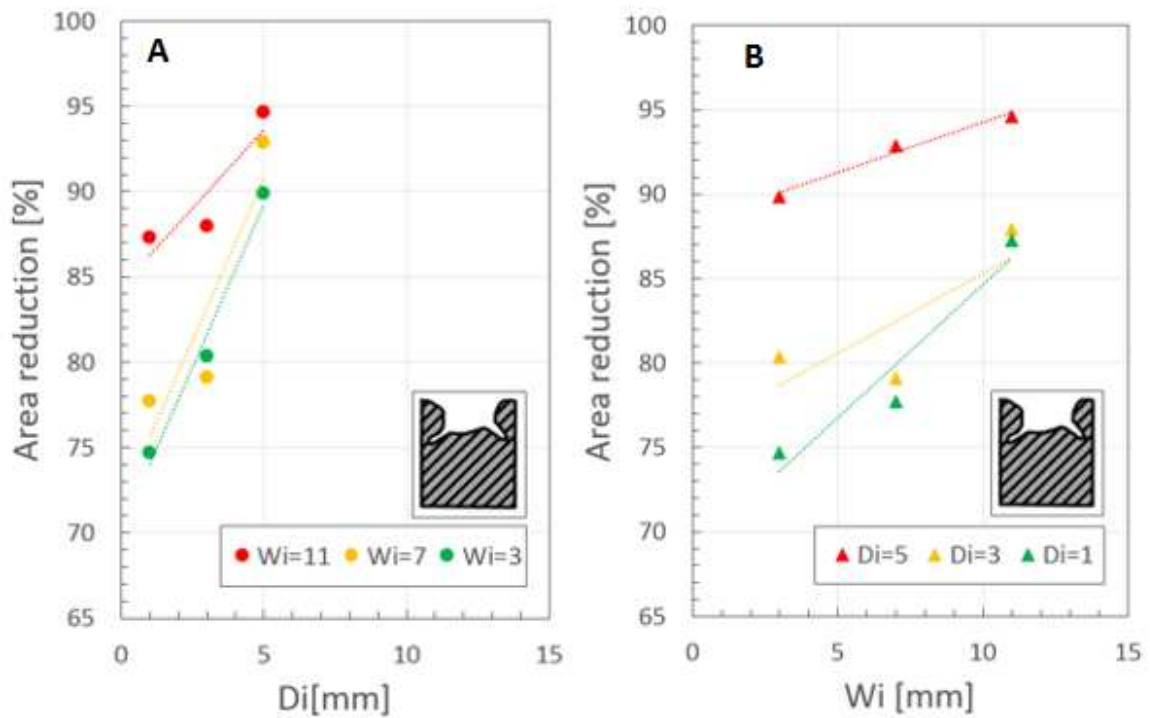


Figure 11: Percentage cross-sectional area reduction of the cavities during the rolling for different initial widths and depths.

In addition, for the given initial widths, the percentage of area reduction increases with the D/W aspect ratio as shown in Figure 12 where defects with different initial width are presented with different colours and symbols. Comparable results are found for the buckling effect presented in Figure 9, where the area reduction effect is more pronounced for wider initial defects.

2007)(Lee S.-L., 2008; Merwin, 2007)(Lee S.-L., 2008; Merwin, 2007)(Lee S.-L., 2008; Merwin, 2007)(Lee S.-L., 2008; Merwin, 2007). Additionally, the present research reports, for the first time, the surface defect evolution for a high-Si electrical steel that is widely used in electrical applications due to its specialised magnetic properties.

The analysis of the micrographs in the transversal cross-section shows that cavities with the same initial width and increasing initial depth resulted in narrower final defects (Figure 5d-f). This is because deeper cavity sides undergo more buckling which reduces the defect width. This phenomenon is presented in Figure 13 where the initial and final outlines of two cavities (B2 and B3) are shown by dashed and solid lines respectively. The cavities were both machined to have an identical width, but B3 is 40% deeper than B2. It is noticeable that the greater the depth to width ratio (D/W) prevented the material from the bottom of the block to flow towards the middle of cavity (Figure 13b) forming a narrow final defect. Conversely, the material was free to spread towards the middle of cavity resulting in a more open final configuration (Figure 13a) for the cavity with a smaller ratio.

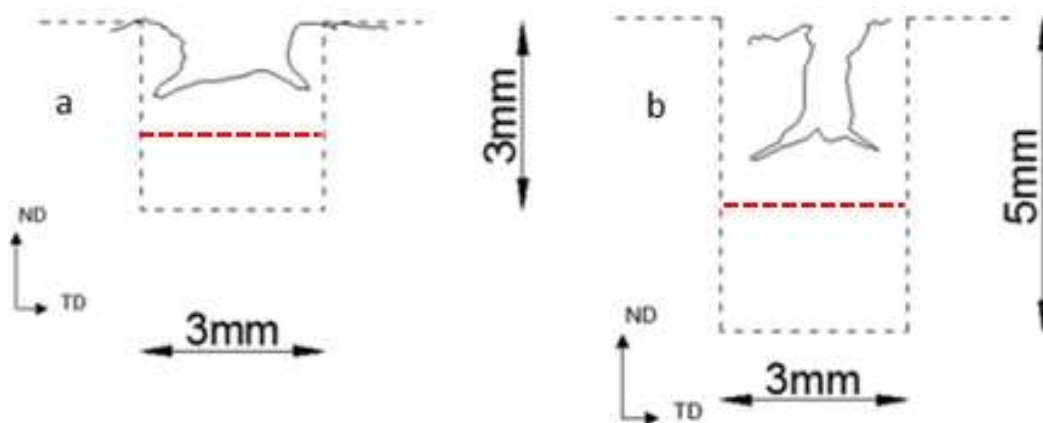


Figure 13: Transversal sections of the defects (a) B2 and (b) B3 showing effect of the initial depth on the evolution mechanism. The dashed line represents the initial cavity shape, the solid line is the final shape after rolling. Red dashed lines indicate a theoretical depth level reduced by 40%, the global value of the deformation of the sample.

In case of a constant initial depth, a smaller depth to width aspect ratio results in shallower final defect (Figure 14). The material at the middle section of the cavity base is less restricted by the side walls in a wider cavity (Figure 14a) resulting in a greater bulging effect of the bottom, and, as a consequence, a shallower final depth. This dependence is shown in Figure 10 where the changes in the measured final depth for the given initial depth are presented against the D/W ratio.

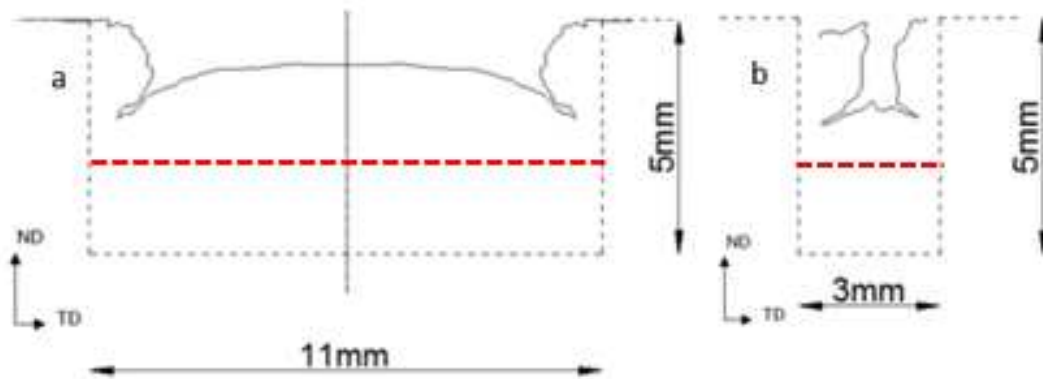


Figure 14: Transversal section of the defects D3 (a), and B3 (b). The dashed line represents the initial defect shape, the continuous line represents the final defect section after the rolling. Red dashed lines indicate a theoretical depth level reduced by 40%

It is interesting to note that all the defects were reduced by more than 50% in depth, although the global thickness reduction applied to the block was only 40%. This is valid for both the depths measured (D_f and D_{fc}). The theoretical depth of the defects after 40% thickness reduction is shown by broken red lines in Figures 13 and 14 indicating that the defects final depths are less than the theoretical assumption. The reason of the more pronounced depth reduction of the defects in the shallower point (D_f) is the bulging of the material from the bottom of the defect. The more pronounced depth reduction measured in the crevices (D_{fc}) is the transversal spreading of the material due to the buckling of the lateral sides of the defect. This is because the material transversal elongation results in a vertical contraction of the material near to the defect reducing its depth.

The analysis of the area reduction in Figure 11 showed that deeper and wider cavities experience the largest area reduction after deformation. Again, this is due to the buckling of the side walls and the

spreading of the material from the bottom towards the middle of the cavities. These effects are presented in Figure 15, where the buckling of the lateral sides and the spreading from the bottom of the defect are indicated with red and blue arrows respectively.

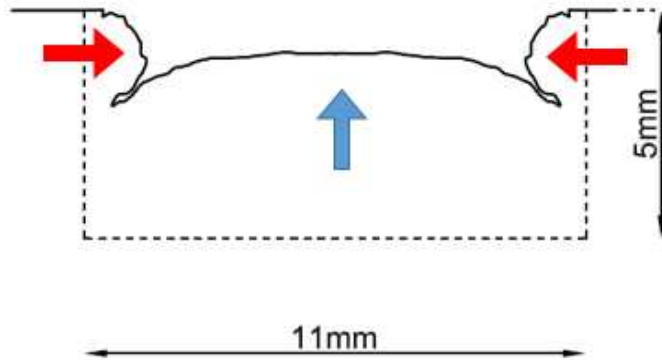


Figure 15: Buckling effect of the lateral sides (red arrows), and spreading effect of the material from the bottom of the defect (blue arrow). The continuous and the dashed lines represent the defect before and after rolling respectively.

In addition, the comparison of the slopes of the trend lines representing the reduction in cross-sectional area against initial depth (Figure 11a) and initial width (Figure 11b) shows that an increase of the initial depth has a more pronounced effect in terms of percentage reduction of cross-sectional area than an increase of the initial width. This suggests that the buckling of the lateral sides has a more important effect on the reduction in cross-sectional area than the material bulging from the bottom of the cavity. In fact, the buckling of the lateral sides of the defects is a direct consequence of the compression applied by the roll during rolling, while the spreading of the material from the bottom of the cavity is an indirect response of the material to the compression which generates a material flow within the cavity.

The sensitivity analysis conducted by measuring the buckling effect of the lateral sides and the percentage of area reduction of the defects show similar results. In fact, in both cases higher D/W aspect ratio of the initial cavities resulted in more severe final defects. Similar findings are also reported in the literature (Lee S.-L., 2008). However, when analysing the buckling effect, it was

observed that the initial width of the cavities plays an important role in the buckling of the lateral sides of the defect. It seems that the aspect ratio has a more pronounced effect in wider initial cavities. This is shown in Figure 9 by comparing the higher slope of the trend lines for wider initial defects. This more pronounced effect is analogous to the one observed when measuring the percentage of area reduction shown in Figure 12. This is further confirmation of the strong dependency between area reduction and buckling of lateral sides of the defect.

4.2 Predictive regression equation development

A second order polynomial regression equation, as expressed in (Montgomery, 2013), with three predictor variables (initial width, depth, and length) was used to correlate the initial cavity geometry to the final configuration. The equation can then be used to predict the final defect characteristics with respect to the initial dimensions. Eq.(1) shows the general form of the proposed model wherein W_i , D_i and L_i represent the initial width, depth and length, respectively.

$$Y = \beta_0 + \beta_1 \cdot W_i + \beta_2 \cdot D_i + \beta_3 \cdot L_i + \beta_4 \cdot W_i^2 + \beta_5 \cdot D_i^2 + \beta_6 \cdot L_i^2 + \beta_7 \cdot W_i \cdot D_i + \beta_8 \cdot W_i \cdot L_i + \beta_9 \cdot L_i \cdot D_i \quad (1)$$

The dependent variable Y was used to represent the final width, depth or length of the defect after rolling at a given condition. The regression coefficient β_0 shows the intercept of the surface described by the regression equation. The linear and quadratic contributions of each predictor variable are the coefficients β_1 - β_6 . Additionally, the last three coefficients (β_7 , β_8 , β_9) determine the expected change in Y due to the interaction between initial geometrical parameters W_i , D_i , and L_i .

Figure 16 shows the effect of initial dimensional variables of the cavities on the measured final length and compares this to the model prediction. According to the figure, the final length is almost independent of the initial width and depth of the defects and it is mostly influenced by the initial length of the defect. Eq.(2-4) show the developed functions to predict the final length, width, and depth, respectively, according to the given variables and the generic polynomial of Eq.(1). The regression coefficients β_i were replaced by the terms a-g, m and n, o and the subscripts W,D,L

indicate whether the parameters were used to predict the final length, width or depth of the defects respectively. The regression coefficients a-o were calibrated using the least square method available on Matlab to minimise the sum of squared residuals between the measured and predicted results for each data point.

$$L_f = a_L + b_L \cdot W_i + c_L \cdot D_i + d_L \cdot L_i + e_L \cdot W_i^2 + f_L \cdot D_i^2 + g_L \cdot L_i^2 + m_L \cdot W_i \cdot D_i + n_L \cdot W_i \cdot L_i + o_L \cdot L_i \cdot D_i \quad (2)$$

$$W_f = a_W + b_W \cdot W_i + c_W \cdot D_i + d_W \cdot L_i + e_W \cdot W_i^2 + f_W \cdot D_i^2 + g_W \cdot L_i^2 + m_W \cdot W_i \cdot D_i + n_W \cdot W_i \cdot L_i + o_W \cdot L_i \cdot D_i \quad (3)$$

$$D_f = a_D + b_D \cdot W_i + c_D \cdot D_i + d_D \cdot L_i + e_D \cdot W_i^2 + f_D \cdot D_i^2 + g_D \cdot L_i^2 + m_D \cdot W_i \cdot D_i + n_D \cdot W_i \cdot L_i + o_D \cdot L_i \cdot D_i \quad (4)$$

It was found that, for the prediction of the final length (L_f), the coefficients associated with the initial depth and width of the cavities are several order of magnitude smaller than those related to L_i variable. This indicates that initial width and depth have a negligible effect on the final length of the cavities after deformation and this can be predicted using Eq.(5):

$$L_f = a_L + d_L \cdot L_i + g_L \cdot L_i^2 \quad (5)$$

The coefficients determined and the relative confidence intervals constructed at a confidence level of 95% are listed below:

$$a_L = -1.147 \text{ (-2.898, 0.6044)}; \quad d_L = 1.573 \text{ (1.173, 1.972)}; \quad g_L = 0.0014 \text{ (-0.01716, 0.02001)}$$

The Root mean square error (RMSE) is 0.9255.

The solid lines in Figure 16 show the predicted curves for the final length of defects with different initial width and depth values.

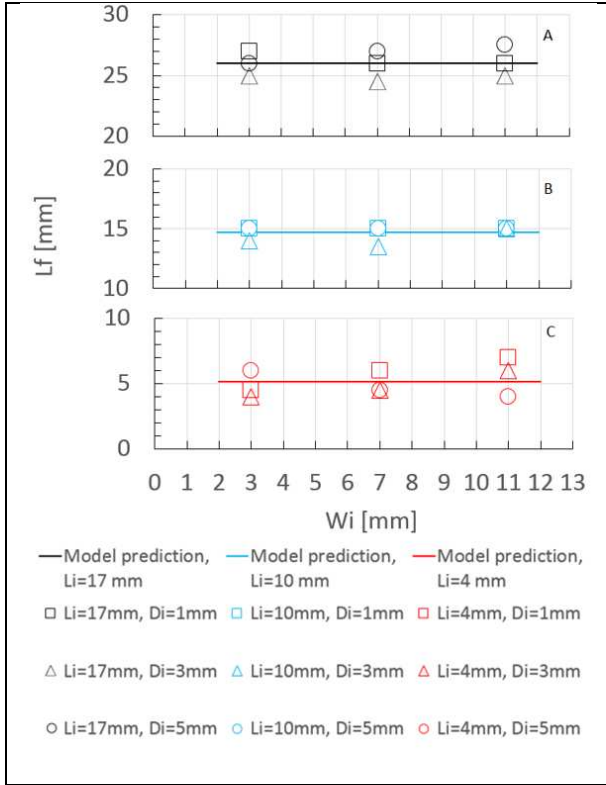


Figure 16: Experimental measurement and prediction of the final length for defects with different initial depths and widths.

A similar procedure was used to obtain the required functions to predict final width and depth values of the cavities. A least-square technique was applied to determine the regression coefficients and those with a negligible effect were excluded from the respective equations. The calibration process showed that the effect of the initial length on the evolution of the cavities can be ignored for the transverse (width) and normal (depth) directions. According to the least-square fitting results, the interactive summation terms (associated with m , n , and o) were found to be negligible compared with the other coefficients for the W_f function (Eq.(6)). It was also found that the quadratic terms have negligible effect in the prediction function for D_f . Consequently, a linear function was obtained simply with different slopes depending on the initial depth of the defects (Eq.(7)).

$$W_f = a_w + b_w \cdot W_i + e_w \cdot W_i^2 + f_w \cdot D_i^2 \quad (6)$$

The coefficients determined and the relative confidence intervals constructed at a confidence level of 95% are listed below:

$a_w = -0.9289$ (-2.06, 0.2027); $b_w = 1.093$ (0.7209, 1.464); $e_w = -0.07458$ (-0.09439, -0.05478);
 $f_w = -0.01052$ (-0.03672, 0.01568)

The Root mean square error (RMSE) is 0.4964.

$$D_i = a_D + b_D \cdot W_i + c_D \cdot D_i + m_D \cdot W_i \cdot D_i = (a_D + c_D \cdot D_i) + (b_D + m_D \cdot D_i) \cdot W_i \quad (7)$$

The coefficients determined and the relative confidence intervals constructed at a confidence level of 95% are listed below:

$a_D = -0.02528$ (-0.4019, 0.3513); $b_D = 0.4342$ (0.3251, 0.5433); $c_D = 0.008633$ (-0.04013, 0.0574);
 $m = -0.03424$ (-0.04803, -0.02046)

The Root mean square error (RMSE) is 0.1912.

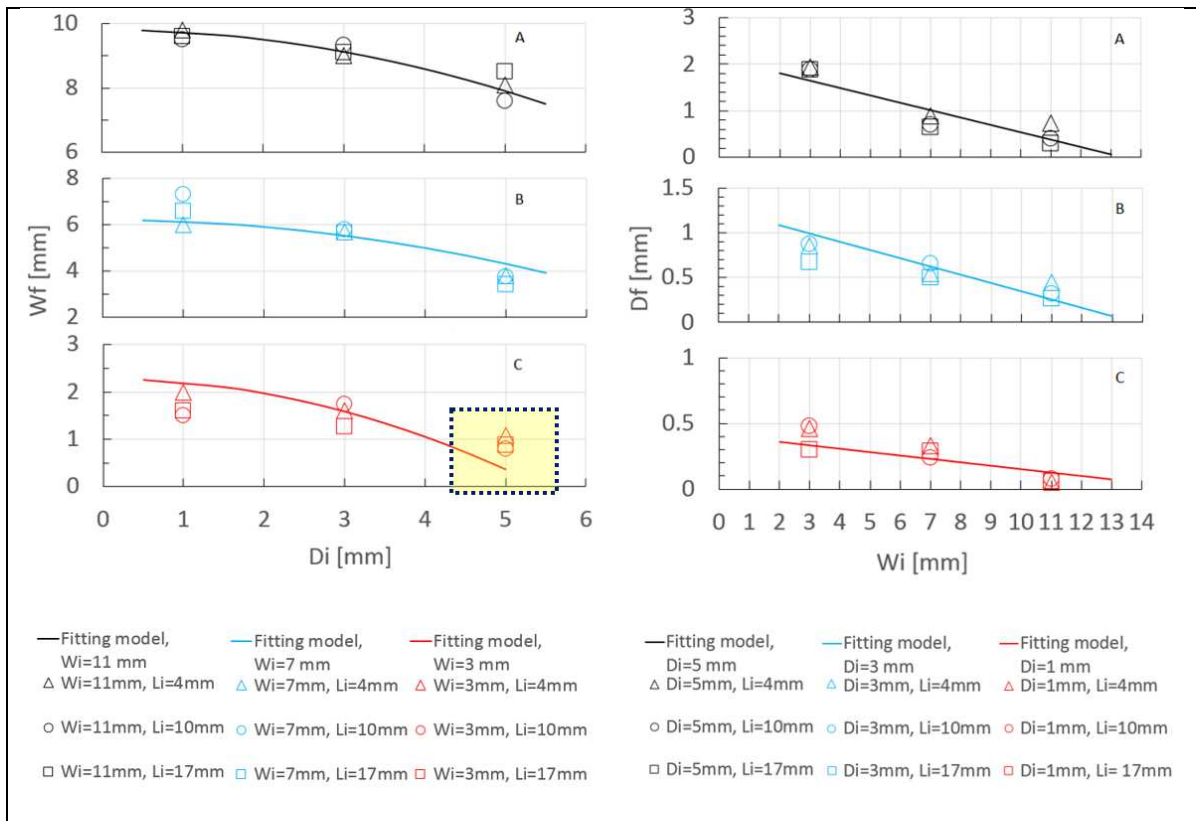


Figure 17: Left) final width prediction, for different initial depths and lengths, Right) final depth prediction, for different initial widths and lengths.

Figure 17 shows the effect of initial dimensional variables of the cavities on the measured final width (Figure 17-left) and final depth (Figure 17-right) and compares this to the model prediction. In general, a good match is found between the model and the experimental values. However, the model is under-predicting the final width for short and deep cavities as it is highlighted in Figure 17c-left). A possible explanation for this may be that the presence of oxide inside the cavities, visible in Figure 7, may have prevented the defect to be further reduced in width during the rolling.

Considering the good match encountered, equations can be used to predict final defect dimension of known initial cavities dimensions.

CONCLUSION

The selected design methodology with three control parameters (D, L, and W) provided a better insight into the cavity evolution mechanisms in three dimensions compared with the previous

studies where only cylindrical holes with two control parameters were used (Lee S.-L., 2008). The results obtained from this study can be summarised as follows:

- The initial length of the surface defects does not play a crucial role in the evolution of the final defects.
- The key geometrical parameters of the initial cavity that predominantly determine the final defect dimensions are the width and the depth.
- The interaction between lateral vertical sides and the bottom surface of the defects is key, with wider initial cavities forming shallower final defects, whereas deeper ones forming narrower final features.
- The buckling of the side walls (both terminal and lateral) is a critical phenomenon that leads to entrapment of the oxide layers within the cavity and leads to crevices at the former bottom corners. Deeper initial cavities result in a more pronounced buckling whereas those initially with a depth of up to 1 mm were essentially eliminated.
- For a given initial depth, the final depth of the defects is found to increase linearly with the initial cavity depth to width aspect ratio.
- Deeper and wider initial cavities are more reduced in terms of percentage of cross-sectional area, and this reduction is mainly caused by the buckling of the lateral sides of the cavities.
- Predictive equations of the final length, width, and depth in function of initial dimensions were developed and showed that:
 - The initial length does not play a major role in determining the final width and depth.
 - There is a non-linear relationship between the final width and the initial depth.
 - The final depth decreases linearly with the initial width.
- The developed technique can be used to develop predictive equations of the final defect dimension of measured initial cavities present on the surfaces of blocks subjected to hot rolling.

ACKNOWLEDGMENT

The project was partly funded by Tata Steel Europe. Technical support of Tata Steel Europe is also greatly acknowledged.

REFERENCES

- Hum, B., Colquhoun, H.W., Lenard, J.G., 1996. Materials Processing Technology Measurements of friction during hot rolling of aluminum strips.
- Krzyzanowski, M., Beynon, J.H., Farrugia, D.C.J., 2009. Oxide Scale Behaviour in High Temperature Metal Processing.
- Lee S.-L., C.J., 2008. Deformation analysis of surface defect on hot rolling by 3-D FEM simulation. Rev. Metall. Cah. D'Informations Tech. 105, 127–135+III–IV. doi:10.1051/metal:2008025
- Lenard, J.G., 1990. An Experimental Study of Boundary Conditions in Hot and Cold Flat Rolling 279–282.
- Lenard, J.G., Barbulovic-nad, L., 2002. The Coefficient of Friction During Hot Rolling of Low Carbon Steel 124, 840–845. doi:10.1115/1.1454106
- Merwin, M., 2007. Evolution of Artificially Induced Slab Imperfections Through Hot and Cold Rolling.
- Moir, S., Preston, J., 2002. Surface defects - evolution and behaviour from cast slab to coated strip. J. Mater. Process. Technol. 125, 720–724.
- Montgomery, D.C., 2013. Design and analysis of experiments. John Wiley & Sons, Inc.
- Munther, P.A., Lenard, J.G., 1999. The effect of scaling on interfacial friction in hot rolling of steels 88, 105–113.

- Shainu, S., T.K.Roy, B.K.Dey, R.K.Sharma, N.C. Gorain, S.Dhar & C.V.Sastry, 2008. Study on Slab Surface Defects and Generation of FeO Type Slivers in Hot Rolled Coils. Tata Steel Ltd. Jamshedpur.
- Vlado, M., Bidulský, R., Gulová, L., Machová, K., Bidulská, J., Valíček, J., Sas, J., 2011. The Production of Cracks Evolution in Continuously Cast Steel Slab. High Temp. Mater. Process. 30, 105–111. doi:10.1515/htmp.2011.014
- Yu, H., Liu, X., Ren, X., 2008. Behaviour of Longitudinal Cracks on Slab Surfaces in V-H Rolling Processes 2, 537–544. doi:10.2374/SRI07SP066-79-2008-xx
- Záhumenský, P., Merwin, M., 2008. Evolution of artificial defects from slab to rolled products. J. Mater. Process. Technol. 196, 266–278. doi:10.1016/j.jmatprotec.2007.05.045
- Zeze, M., Tanaka, A., Tsujino, R., 2001. Formation mechanism of sliver-type surface defect with oxide scale on sheet and coil. Tetsu to Hagane 87, 85–92. doi:10.2355/tetsutohagane1955.87.2_85